analytical chemistry

pubs.acs.org/ac Article

Noninvasive Bioluminescence Imaging of Matrix Metalloproteinase-14 Activity in Lung Cancer Using a Membrane-Bound Biosensor

Feng Tian,[§] Yan Chen,[§] Wuping Wang, Jipeng Zhang, Tao Jiang,* and Qiang Lu*

Cite This: *Anal. Chem.* 2021, 93, 8739−8745 Read Online

ACCESS | Metrics & More | Article Recommendations | Supporting Information

ABSTRACT: Matrix metalloproteinase-14 (MMP-14) plays a crucial role in the cancer migration and metastasis by guiding the extracellular matrix remodeling and cell motility. Despite increasing efforts have been taken to develop methodology for measuring MMP-14 expression, there is a lack of tools capable of monitoring the MMP-14 dynamic activity with high temporal and spatial resolution in living cells and animals. Here, we describe the design of Gaussia luciferase (Gluc)-based membrane-bound biosensor for efficient visualization of MMP-14 activity. The epidermal growth factor (EGF) induced significant luciferase changes in the biosensor-transfected lung cancer cells. Deletion of the transmembrane domain in the mutant biosensor or treatment with an MMP-14 inhibitor, tissue inhibitor of metalloproteinase-2 (TIMP-2), relieved the EGF-induced luciferase activation, suggesting that MMP-14 functions at the cell surface to result in luciferase changes. Moreover, utilizing this biosensor, the bioluminescence signals activated by MMP-14 enabled clear visualization of MMP-14-positive lung tumors in animal models. Our results indicated this biosensor is an effective probe for quantitatively monitoring proteolytic activities in live cells and mouse models. These findings offer the general design of biosensors as an adaptable tool for studying various membrane-anchored proteases in biological models.

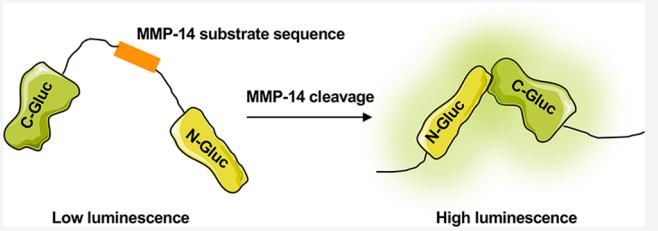

INTRODUCTION

At present, malignant tumors have jumped to the top of the cause of human death, and lung cancer mortality has ranked the first in both male and female malignancies.[1] Nonsmall-cell lung cancer (NSCLC) accounts for about 80% of the total number of lung cancers. More than 50% of typical NSCLC cases are already diagnosed at an advanced stage.[2] For most NSCLC patients, chemotherapy is the main treatment but the prognosis is still poor. Tumor invasion and metastasis are extremely complicated processes. If tumor cells have the ability to invade and metastasize, they must first break through the barrier of the extracellular matrix and have the potential for their own movement.[3] Matrix metalloproteinases (MMPs) are the major zinc-dependent proteolytic enzymes that degrade extracellular matrix and play an important role in the process of tumor invasion and metastasis.[4,5] At present, there are at least 24 types of human MMPs. Based on the sequence similarity and substrate specificity, MMPs can be divided into six categories: collagenases (MMP-1, 8, 13, and 18), gelatinases (MMP-2, 9), matrix-degrading enzymes (MMP-3, 10, and 11), matrilysins (MMP-7, 26), membrane-type MMP (MMP-14, 15, 16, 17, 24, and 25), and other MMPs (MMP-12, 19, 20, 21, 23, 27, and 28).[6,7] Among these enzymes, MMP-14, also known as membrane-type 1 matrix metalloproteinase (MT1-MMP), is considered to be the most dominant member of the MMP family that controls tumor cell behavior.[8] Moreover, MMP-14 is the first member of the membrane-type MMP family to be discovered and is one of the most closely related enzymes in the MMP family that involved in tumor invasion and metastasis especially in NSCLC.[9−11]

Given the significance of MMP-14 in the wide biological functions including tumor development and multiple signaling pathways, increasing efforts have been taken to explore tools for detecting MMP-14 expression. Molecular imaging techniques that employ different imaging modalities have been emerged as an attractive strategy for noninvasively monitoring MMP proteolytic activity in living subjects. To date, various kinds of imaging probes targeting MMP-14 have been developed and tested in tumor cells and animal models. These probes have included near-infrared dye-quencher pair-based fluorogenic probe for fluorescence imaging,[12] MMP-14 substrate-binding peptide for dual positron emission tomography and fluorescence imaging,[13] and a quantum-dot-based fluorescence resonance energy transfer nanosensor for MMP-14 activity profiling.[14] Despite these efforts, to our best knowledge, there have been few activatable bioluminescence probe to dynamically monitor MMP-14 activity with high temporal and spatial resolution in living cells, especially in

Received: December 10, 2020
Accepted: May 30, 2021
Published: June 11, 2021

https://doi.org/10.1021/acs.analchem.0c05189
Anal. Chem. 2021, 93, 8739−8745

living animals. The extremely low background and high sensitivity of bioluminescent reporters provide great advantages for *in vivo* imaging.

In this study, we demonstrated the design and characterization of a membrane-bound form of the Gaussia luciferase (Gluc) reporter for efficient visualization of MMP-14 activity. Gluc, derived from the copepod Gaussia princeps, is the smallest (185 amino acids) luciferase that utilizes coelenterazine as a substrate and emits a bioluminescence signal.[15] Compared to other luciferase such as firefly luciferase (Fluc) or renilla luciferase (Rluc), Gluc is ∼2000-fold more sensitive when expressed in mammalian cells. However, Gluc protein is naturally secreted extracellularly, which significantly attenuates the in vivo bioluminescence signal.[16] To overcome this limitation, we added a platelet-derived growth factor receptor (PDGFR) transmembrane domain to the C-terminus of Gluc so that the MMP-14 reporter could be anchored at the cell membrane. The MMP-14 protease recognition sequence was inserted into the circularly permuted (CP) Gluc protein to generate the MMP-14 membrane-bound reporter. Utilizing this biosensor, MMP-14 activity was dynamically visualized in live cells and tumor-bearing mice with high sensitivity. Our results indicated the general applicability of the reporter as an adaptable tool for studying the membrane-bound proteases in various biological models.

MATERIALS AND METHODS

Plasmids and Biosensor Construction. To construct the biosensor, the Gluc gene was CP at residue 79, 93, or 106 based on the secondary structure prediction. A 12-amino acid sequence (GRIGFLRTAKGG) for the MMP-14 cleavage site was designed for the biosensor. For plasmid permuted at residue 79, DNA encoding a Met-(79-185)- GRIGFLRTAKGG-(17-78)-Val fusion protein was cloned into the pDisplay vector (Invitrogen) using BglΠ/PstI sites for mammalian cell expression. For plasmid permuted at residue 93 or 106, DNA encoding a Met-(93-185)- GRIGFLRTAKGG-(17-92)-Val fusion protein or Met-(106-185)-GRIGFLRTAKGG-(17-105)-Val fusion protein was also cloned into the pDisplay vector. These three constructs were designated as MMP-CP79, MMP-CP93, or MMP-CP106, respectively. Since the residues 1-16 of Gluc is the native signal peptide for Gluc,[17] we only cloned the residues 17-185 of Gluc into the pDisplay vector, which contains a C-terminal PDGFR transmembrane domain for targeting plasma membrane. A mutant biosensor was also constructed by deleting the sequence encoding the PDGFR transmembrane domain by mutated PCR. All of the final constructs were sequenced to ensure correct in sequence.

Cell Culture, Transfection, and Recombinant Adenovirus Generation. Hela, A549, and HKP1 cells were maintained in our laboratory and cultured in Dulbecco's modified Eagle's medium (Gibco, Carlsbad, CA) supplemented with 10% fetal bovine serum (Gibco) and 100 U/mL penicillin/streptomycin (Gibco) at 37 °C under 5% CO_2. For the transfection experiment, the cells were seeded at a density of 3×10^4 on 24-well plates and transfected with the plasmids using the lipofectamine 2000 (Invitrogen) on the next day. For recombinant adenovirus generation, the resulting MMP-CP93 construct was subcloned into a pAvCvSv shuttle vector and cotransfected into HEK293 cells with adenovirus backbone vector pJM17. The adenoviruses expressing MMP-CP93 were produced, designated as Ad-MMP-CP93. As a control, the adenoviruses with only the adenovirus backbone Ad-Mock were also constructed.

In Vitro Measurement of Gluc Activity. The three plasmids encoding the biosensors were used as templates in the TNT SP6 high-yield protein expression system (Promega) according to the manufacturer's instructions. Briefly, 2 μg of plasmid DNA was added to 30 μL of master mix lysate plus 2 μL of FluoroTect green *in vitro* translation labeling system (Promega). Then, the total volume was brought to 50 μL with dH_2O. The 50 μL in vitro translation reaction mixtures were then incubated at 25 °C for 2 h. A total of 15 μL of the reaction mixture was then mixed with 15 μL of a 2× MMP-14 protease buffer with 1 μL of MMP-14 protease (10 U/L). The digest reaction mixtures were incubated at 37 °C for 30 min. A total of 5 μL of the digest reaction mixtures was placed in a 96-well luminometer plate, and luminescence was measured following the addition of 100 μL of luciferase assay reagent using a Glomax 96 microplate luminometer (Promega).

Measurement of Gluc Activity in Cells. For measurement of luciferase activity in cells, the cell lysate in lysis buffer (Promega) was added with the substrate coelenterazine (5 μg/mL, Promega) and the luminescence intensity was immediately measured with a Blight-Glo Luciferase Assay Kit (Promega) using a luminometer instrument (Promega) according to the manufacturer's instructions. The luminescence results were presented as counts per minute (cpm) per μg of protein.

Flow Cytometry Analysis. Hela cells were transfected with the wild-type (WT) biosensor or a mutant biosensor. 24 h later, the cells were washed with phosphate-buffered saline (PBS) and collected by incubating with PBS at room temperature for 5 min. The cells were then incubated with rabbit anti-HA monoclonal antibody (Santa Cruz Biotechnology) on ice for 30 min. The cells were washed and then incubated with fluorescein isothiocyanate-labeled mouse anti-rabbit IgG antibody (Santa Cruz Biotechnology) on ice for 30 min. Finally, the cells were washed and measured by FACS Calibur (BD Bioscience) with CellQuest software.

Animal Model. All animal experiments were approved by the Animal Care and Use Committee of Air Force Medical University. Six week-old female BALB/c nude mice were obtained from Animal Center of the Air Force Military Medical University and maintained on a standard diet at room temperature. Xenografted lung tumor models were prepared by subcutaneous injection of 5×10^7 HKP1 lung cells suspended in 150 μL of PBS into nude mice. When the tumor volume reached about 100 mm^3, the mice were used for in vivo bioluminescence imaging. The animal status was monitored closely throughout the experiment.

***In Vivo* Bioluminescence Imaging.** For the *in vivo* imaging, a total of 10^{11} pfu of Ad-MMP-CP93 viruses in 50 μL of PBS was injected locally into the tumor sites of mice. During the injection and imaging process, the mice were anesthetized with isofluran-mixed oxygen and injected with 200 μg of coelenterazine intraperitoneally 5 min before imaging. The imaging was performed at 0, 1, 3, 6, 12, and 24 h time point after the injection of viruses (n = 6/group). The mice were then scanned using a Xenogen IVIS spectrum (Xenogen, Hopkinton, MA) for 1 min. The images are shown as p/s/cm^2/sr. To inhibit MMP-14 expression, 1 μmol of TIMP-2 inhibitor was injected intratumorally 30 min prior to injection of Ad-MMP-CP93. For quantitative analysis, regions of interest (ROI) were drawn over tumors and muscle, and the average signal for each area was measured.

https://doi.org/10.1021/acs.analchem.0c05189
Anal. Chem. 2021, 93, 8739−8745

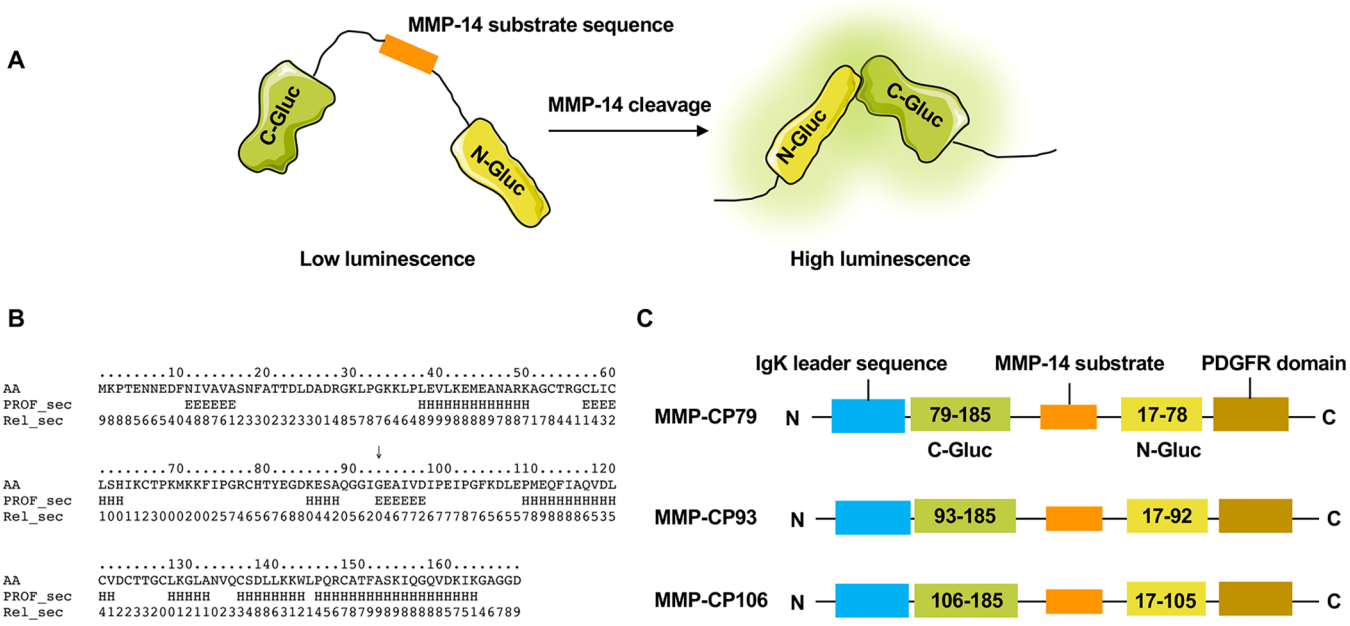

Figure 1. Design of the biosensor for MMP-14 imaging. (A) Schematic of the MMP-14 biosensor containing an N-terminus coding for the C-Gluc domain, a C-terminus coding for the N-Gluc domain, and an MMP-14 substrate sequence. (B) Amino acid sequence of Gluc (the N-terminal amino acid 1−16 for the signal peptide was not included) and secondary structure prediction by CDM algorithm. AA, amino acid; PROF_sec, predicted secondary structure; Rel_sec, reliability index for PROF_sec (0 = low to 9 = high); E = extended (sheet); and H = helix. (C) Schematic of three genetically encoded variants of MMP-14 biosensors, MMP-CP79, MMP-CP93, and MMP-CP106. The Gluc gene was CP at residue 79, 93, or 106 based on the secondary structure prediction. The MMP-14 substrate was inserted into the respective residue site. The fused protein was subcloned into a pDisplay vector, which contains an N-terminal IgK leader sequence for targeting the secretory pathway and a C-terminal PDGFR transmembrane domain for targeting the plasma membrane.

Immunohistology. HKP1 tumor slides were frozen in optimal cutting temperature embedding medium, dried, and fixed with cold acetone for 30 min. Cryosections were cut into 4 μm slices. After blocking with 10% BSA for 1 h, the sections were incubated with mouse anti-MMP-14 antibody (Santa-Cruz Biotechnology) at room temperature for 60 min and then incubated with Alexa Fluor 568 rabbit anti-mouse secondary antibody (SantaCruz Biotechnology). Finally, the slices were stained with 4′,6-diamidino-2-phenyl-indole (DAPI)-containing mounting medium under an epifluorescence microscope (Olympus, X81).

Statistical Analysis. All quantitative data were expressed as mean ± standard deviation (SD). The statistical analyses were performed on Graphpad prism and using Student's t test. The *P*-values (***: $P < 0.001$, **: $P < 0.01$; *: $P < 0.05$) denoted different levels of statistical significance.

RESULTS

Design of the MMP-14 Membrane-Bound Biosensor. To generate a sensitive biosensor for detecting MMP-14 activity, a twelve-amino acid sequence (GRIGFLRTAKGG) for the MMP-14 cleavage site was inserted into the CP Gluc gene, which consists of an amino-terminal domain coding for the carboxyl terminus of Gluc (C-Gluc) and carboxyl-terminal domain for the amino terminus of Gluc (*N*-Gluc) (Figure 1A). Since MMP-14 is directed toward the extracellular plasma membrane, the signal peptide (residues 1−16) of native Gluc was deleted and the cDNA encoding the CP Gluc was subcloned into pDisplay plasmid vector, which contains an N-terminal IgK leader sequence for targeting the secretory pathway and a C-terminal PDGFR transmembrane domain for targeting the plasma membrane. In this construct, we assumed that there is no luciferase signal in the absence of MMP-14 activity. When MMP-14 is present on the cell surface, active MMP-14 would cleave at the substrate site of the biosensor and reconstitute the CP Gluc, which result in an increase in the luminescence signal that can be detected using a bioluminescence imaging instrument.

To ensure that CP Gluc could be successfully reconstituted, three different structurally tolerant Gluc sites were tested for the insertion of the MMP-14 substrate site according to the secondary structure prediction of GLuc using the CDM algorithm.[18] The three cut sites were at 79, Gly93, and 106, which were all within the regions of unstructured Gluc proteins sequence (amino acids 65−109, Figure 1B). Accordingly, these three genetically encoded variants of MMP-14 biosensors, designated as MMP-CP79, MMP-CP93, and MMP-CP106, were constructed with linkage of the MMP substrate sequence (Figure 1C).

***In Vitro* Characterization of the MMP-14 Biosensor.** To determine whether the luciferase activity of the three MMP-14 biosensors was restored in the presence of an MMP-14 enzyme, the luciferase signal was evaluated *in vitro* by incubating these biosensors with recombinant MMP-14 protease in cell-free translation reactions. All three biosensors were activated upon MMP-14 digest as demonstrated by an obvious increase in luciferase activity (Figure 2A). Among them, MMP-CP93 showed the highest fold increase in luciferase and therefore was chosen for our subsequent study (Figure 2B).

To further assess the performance of the MMP-CP93 biosensor, the MMP-CP93 was incubated with different concentrations (0, 10, 20, 40, and 80 nM) of MMP-14 protease in the presence or absence of the MMP-14 inhibitor,

https://doi.org/10.1021/acs.analchem.0c05189
Anal. Chem. 2021, 93, 8739−8745

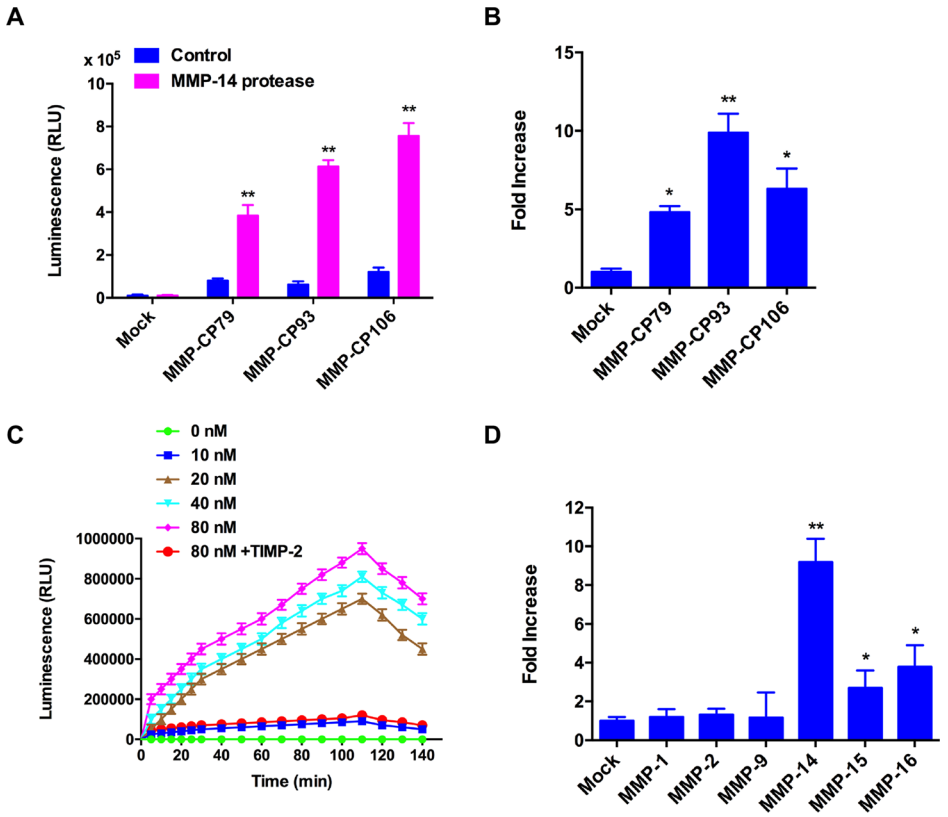

Figure 2. In vitro characterization of the MMP-14 biosensor. (A) 2× MMP-14 protease buffer was diluted 1:1 in cell-free translation reactions with 10 U MMP-14 protease and incubated at 30 °C for 30 min. Then, the luminescence was measured. (B) Fold change in luminescence in MMP-14 protease-treated cells compared with the untreated cells in (A). Results were representative data from three independent experiments. (C) Luminescence kinetic spectra of MMP-CP93 in the presence of different concentrations (0, 10, 20, 40, and 80 nM) of MMP-14 protease or MMP-14 inhibitor TIMP-2 (40 nM) following incubation at 37 °C for 140 min. (D) Luminescence activation of MMP-CP93 in a solution containing various MMPs following incubation at 37 °C for 1 h. *P < 0.05, **P < 0.01 compared with the mock group.

tissue inhibitor of metalloproteinase-2 (TIMP-2). As shown in Figure 2C, the recovery of luminescence signals depended on the concentrations of MMP-14. The luminescence was found to increase gradually and reach a maximum 110 min after incubation with MMP-14 protease, and then, the signal intensity gradually decreased. The plots clearly indicate that MMP-14 was able to activate luminescence signals of MMP-CP93 up to 10-fold at the 80 nM concentration. The activation was remarkably inhibited in the presence of an MMP inhibitor TIMP-2, indicating the selectivity of this biosensor. The specificity of MMP-CP93 was further evaluated by incubating MMP-CP93 with different MMPs including MMP-1, MMP-2, MMP-9, MMP-14, MMP-15, and MMP-16. As shown in Figure 2D, the luciferase activity was significantly higher when incubated with MMP-14 than with other MMPs. Of note, MMP-15 and MMP-16 also induced moderate increase in the luciferase signal, which may be attributed to the sharing of similar catalytic domains among MMP-14, -15, and -16. Taken together, these results indicate the specific cleavage of the MMP-CP93 biosensor only by MMP-14.

Functional Characterization of the MMP-14 Biosensor in Living Cells. Since MMP-14 is mainly expressed toward the extracellular plasma membrane, we first investigated whether the MMP-CP93 biosensor could be targeted to the cell plasma membrane. Hela cells, which do not express endogenous MMP-14,[19] were transfected with the WT biosensor or a mutant biosensor lacking the PDGFR transmembrane domain. The cells were collected for flow cytometry analysis of the fluorescence using a fluorescein isothiocyanate (FITC)-labeled anti-HA antibody based on the HA tag of the constructs. As shown in Figure 3A, compared with control cells, increased fluorescence was observed in the WT biosensor transfected cells but not in the mutant biosensor-transfected cells. However, after the cells were permeabilized, the mutant biosensor transfected cells showed significant fluorescence signal. The confocal fluorescence microscope images also demonstrated that strong FITC fluorescence staining in the WT biosensor-transfected cells and the permeabilized mutant biosensor-transfected cells but not in nonpermeabilized cells (Supporting Information, Figure S1). These results suggested that the MMP-CP93 biosensor is successfully targeted to the cell membrane.

We next utilized this biosensor to measure the MMP-14 enzyme in living cells. Hela cells were cotransfected with the MMP-CP93 construct and a plasmid expressing WT MMP-14 enzyme. The epidermal growth factor (EGF), an extracellular ligand of EGF receptor (EGFR) family members, was added into the transfected cells for 1 h. The EGF has been reported to trigger tumor invasion by regulating MMP-14 expression.[20] As shown in Figure 3B, a significant increased luciferase signal was observed in the presence of EGF compared with the control group. By contrast, deletion of the PDGFR in the mutant biosensor blocked the EGF-induced luciferase increase, indicating that EGF-induced MMP-14 activation occurred preferentially at the cell membrane. Finally, an endogenous inhibitor of MMP-14, tissue inhibitor of metalloproteinase-2

https://doi.org/10.1021/acs.analchem.0c05189
Anal. Chem. 2021, 93, 8739−8745

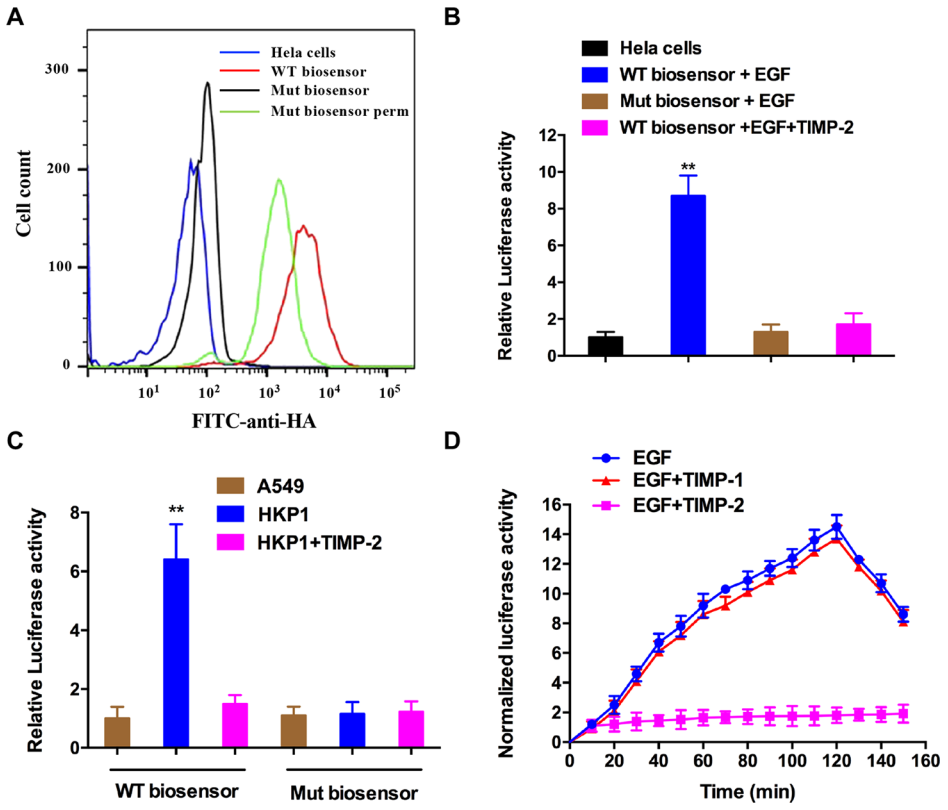

Figure 3. Functional characterization of the MMP-14 biosensor in living cells. (A) Hela cells were transfected with the WT biosensor or a mutant (Mut) biosensor. The cells were stained with FITC-labeled anti-HA antibody and analyzed by flow cytometry. To further study the biosensor targeted to the cell plasma membrane, the Mut biosensor-transfected cells were fixed, permeabilized, and stained with the same antibody. A representative picture from three independent experiments was shown. (B) Hela cells were cotransfected with the MMP-CP93 WT biosensor or Mut biosensor as well as a plasmid expressing WT MMP-14 enzyme. The EGF was added into the transfected cells with or without the TIMP-2 inhibitor for 1 h. The luciferase activities from each transfected group were measured from three independent experiments. $^{**}P < 0.01$ compared with the Hela mock group. (C) WT or Mut biosensor was transiently transfected into A549 or HKP1 cells with or without the TIMP-2 inhibitor. 24 h later, the luciferase activities were measured in each transfected group. $^{**}P < 0.01$ compared with the A549 cell group. (D) MMP-CP93 WT biosensor-transfected A549 cells were treated with 2.5 g/mL TIMP-2 or TIMP-1 for 10 min before EGF stimulation for 150 min. Representative time course of normalized luciferase activity is shown in cells with different treatments.

(TIMP-2), also abolished the EGF-induced luciferase activation in the WT MMP-CP93-transfected Hela cells, which may be attributed to the suppression of the MMP-14 enzyme by the TIMP-2 inhibitor.

To evaluate the ability of the MMP-CP93 biosensor to detect endogenous MMP-14 activity in living cells, the biosensor was transiently transfected into two different lung cancer cell lines: A549 cells that express minimal levels of endogenous MMP-14 and HKP1 cells derived from KP tumor lungs with high MMP-14 expression. The luciferase signal was significantly higher in HKP1 cells compared to that in A549 cells (Figure 3C), indicating that endogenous MMP-14 cleaved the substrate site of the biosensor and restored the luciferase activity. In contrast, the addition of the MMP-14 inhibitor, TIMP-2, caused the decreased luciferase signal in HKP1 cells. However, the mutant biosensor transfected A549 cells or HKP1 cells both showed a low luciferase signal regardless of the presence of TIMP-2. Since EGFR is abundant in the A549 cells, we further explored whether the MMP-CP93 biosensor could monitor the dynamic activation of endogenous MMP-14 in response to EGF stimulation. Time course analysis revealed that a significant luciferase signal increase was observed in A549 cells upon EGF treatment (Figure 3D). Then, the signal reached a maximum 120 min after stimulation with EGF, and then, the luciferase intensity gradually decreased, whereas this EGF-induced luciferase increase was significantly suppressed by TIMP-2 but not TIMP-1 inhibitor, which prefers to target-secreted MMPs.[21] Taken together, these results indicate that our MMP-CP93 biosensor can specifically monitor MMP-14 activity in real-time in living cells.

***In vivo* Imaging of MMP-14 in Tumor-Bearing Mice.** After verifying the feasibility of the MMP-CP93 biosensor *in vitro*, we further investigated its *in vivo* potential application using the tumor-bearing mice models. 5×10^7 HKP1 lung cells were implanted into the flanks of mice to establish the HKP1-tumor-bearing mice. Then, we injected 1×10^{11} pfu adenovirus of MMP-CP93 (Ad-MMP-CP93) into the tumor sites of mice ($n = 6$). *In vivo* bioluminescence imaging was performed over 72 h. As shown in Figure 4A, increased bioluminescence signals were observed in the MMP-14-positive tumor region. It is noted that this biosensor clearly detected early activation of MMP-14 (1 h) and the high bioluminescent signals were maintained up to 24 h in the tumor site and then decreased afterward. In contrast, when a TIMP-2 inhibitor was preinjected intratumorally 30 min before the biosensor injection, the bioluminescent signals were significantly decreased over time. The tumor-to-muscle ratio (T/M ratio) in the ROI demonstrated that the bioluminescent signals gradually increased up to 3 h after the injection of the biosensor and could remain sustained for 24 h and then

https://doi.org/10.1021/acs.analchem.0c05189
Anal. Chem. 2021, 93, 8739−8745

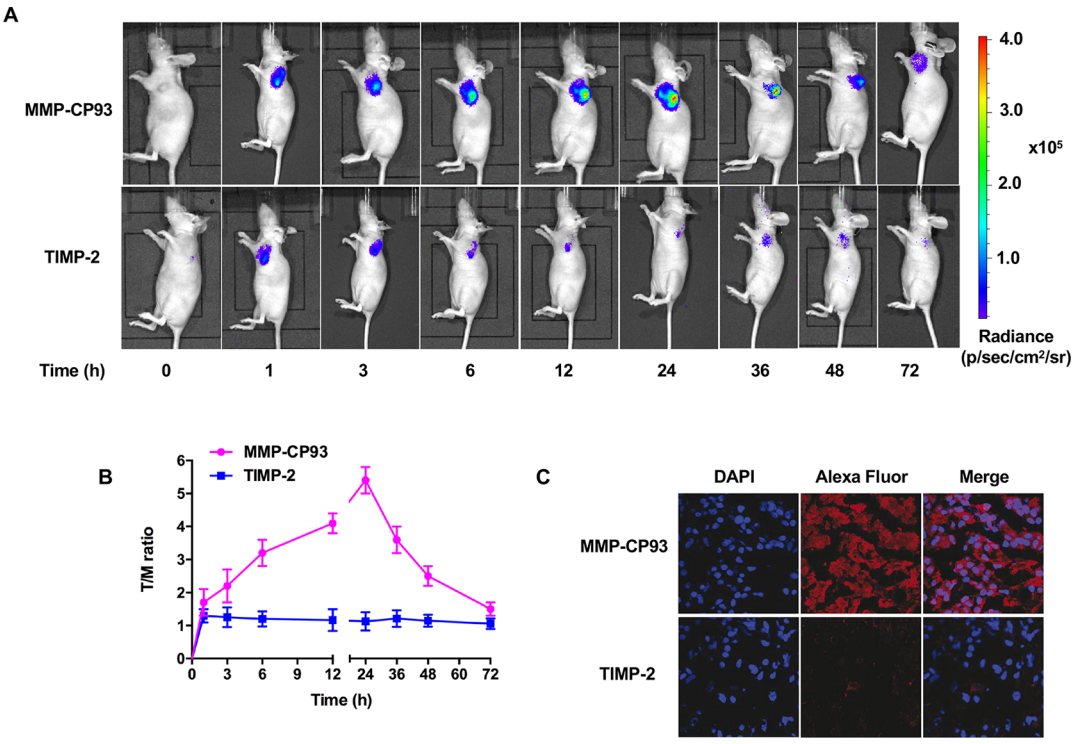

Figure 4. *In vivo* monitoring of MMP-14 expression in tumor-bearing mice. (A) Representative *in vivo* bioluminescence images of HKP1 tumor-bearing mice injected intratumorally with Ad-MMP-CP93 without or with an MMP inhibitor (TIMP-2). Images were acquired at the indicated time points. (B) Ratio of the signal in the ROI of the tumor compared to the muscle region (T/M ratio) analysis of HKP1 tumor in vivo. Means ± SD (n = 6 per group). (C) Representative fluorescence images of tumor sections injected with Ad-MMP-CP93 without or with TIMP-2. Tumor sections were incubated with mouse anti-MMP-14 antibody and then incubated with Alexa Fluor 568 rabbit anti-mouse secondary antibody. The sections were counterstained with DAPI. Scale bar, 50 μm.

subsequently decreased to a low level at 72 h time point (Figure 4B), whereas the signals were inhibited at all time points when the activity of MMP-14 was suppressed by the TIMP-2 inhibitor. The *ex vivo* imaging of the tumors at 24 h postinjection confirmed that the strong luminescence signal was observed in the Ad-MMP-CP93-alone treatment group but not in the TIMP-2 inhibitor cotreatment tumors (Supporting Information, Figure S2). Moreover, microscopic imaging of tumor sections demonstrated that the obvious fluorescence signal colocalized in the tumor sections, which showed high expression of MMP-14. In contrast, the sections that simultaneously injected with TIMP-2 exhibited a low fluorescence signal (Figure 4C). Taken together, these results suggest that the present MMP-CP93 biosensor is applicable to in vivo sensing of MMP-14 expression in real-time.

CONCLUSIONS

In this study, we described the design of an MMP-14-specific membrane-bound biosensor and demonstrated the capability of using this biosensor to monitor the MMP-14 expression in living cells and animals. Our findings provide a new type of membrane-anchored protease-targeting biosensor for visualizing the spatiotemporal activity of membrane-tethered MMP enzymes. It will eventually improve our understanding of the role of membrane-related proteases in cancer cell biology and enhance the screening capabilities of specific protease inhibitors for drug development.

ASSOCIATED CONTENT

Supporting Information

The Supporting Information is available free of charge at https://pubs.acs.org/doi/10.1021/acs.analchem.0c05189.

Confocal images of the cell surface localization of the MMP-CP93 biosensors and bioluminescence images of dissected tumors (PDF)

AUTHOR INFORMATION

Corresponding Authors

Qiang Lu − *Department of Thoracic Surgery, Tangdu Hospital, Air Force Medical University, Xi'an 710038, China*; orcid.org/0000-0001-6004-9242; Email: luqiang@fmmu.edu.cn

Tao Jiang − *Department of Thoracic Surgery, Tangdu Hospital, Air Force Medical University, Xi'an 710038, China*; Email: jiangtaochest@163.com

Authors

Feng Tian − *Department of Thoracic Surgery, Tangdu Hospital, Air Force Medical University, Xi'an 710038, China*

Yan Chen − *Department of Oncology, Xijing Hospital, Air Force Medical University, Xi'an 710032, China*

Wuping Wang − *Department of Thoracic Surgery, Tangdu Hospital, Air Force Medical University, Xi'an 710038, China*

Jipeng Zhang − *Department of Thoracic Surgery, Tangdu Hospital, Air Force Medical University, Xi'an 710038, China*

Complete contact information is available at: https://pubs.acs.org/10.1021/acs.analchem.0c05189

https://doi.org/10.1021/acs.analchem.0c05189
Anal. Chem. 2021, 93, 8739−8745

Author Contributions

[§]F.T. and Y.C. contributed equally to this work.

Notes

The authors declare no competing financial interest.

■ ACKNOWLEDGMENTS

This work was supported by the National Natural Science Foundation of China (no. 81872265).

■ REFERENCES

(1) Siegel, R. L.; Miller, K. D.; Jemal, A. *Ca-Cancer J. Clin.* **2020**, *70*, 7−30.
(2) Sim, W. C.; Loh, C. H.; Toh, G. L.-X.; Lim, C. W.; Chopra, A.; Chang, A. Y. C.; Goh, L. L. *Lung Cancer* **2018**, *124*, 154−159.
(3) Pickup, M. W.; Mouw, J. K.; Weaver, V. M. *EMBO Rep.* **2014**, *15*, 1243−1253.
(4) Visse, R.; Nagase, H. *Circ. Res.* **2003**, *92*, 827−839.
(5) Deryugina, E. I.; Quigley, J. P. *Cancer Metastasis Rev.* **2006**, *25*, 9−34.
(6) Bode, W.; Fernandez-Catalan, C.; Grams, H. T. F.; Maskos, H. N. K.; Nagase, H.; Maskos, K. *Cell. Mol. Life Sci.* **1999**, *55*, 639−652.
(7) Klein, T.; Bischoff, R. *Amino Acids* **2011**, *41*, 271−290.
(8) Remacle, A. G.; Rozanov, D. V.; Baciu, P. C.; Chekanov, A. V.; Golubkov, V. S.; Strongin, A. Y. *J. Cell Sci.* **2005**, *118*, 4975−4984.
(9) Wang, Y.-z.; Wu, K.-p.; Wu, A.-b.; Yang, Z.-c.; Li, J.-m.; Mo, Y.-l.; Xu, M.; Wu, B.; Yang, Z.-x. *Tumor Biol.* **2014**, *35*, 9815−9821.
(10) Stawowczyk, M.; Wellenstein, M. D.; Lee, S. B.; Yomtoubian, S.; Durrans, A.; Choi, H.; Narula, N.; Altorki, N. K.; Gao, D.; Mittal, V. *Neoplasia* **2017**, *19*, 55−64.
(11) Pekkonen, P.; Alve, S.; Balistreri, G.; Gramolelli, S.; Tatti-Bugaeva, O.; Paatero, I.; Niiranen, O.; Tuohinto, K.; Perälä, N.; Taiwo, A.; Zinovkina, N.; Repo, P.; Icay, K.; Ivaska, J.; Saharinen, P.; Hautaniemi, S.; Lehti, K.; Ojala, P. M. *Elife* **2018**, *7*, No. e32490.
(12) Zhu, L.; Zhang, F.; Ma, Y.; Liu, G.; Kim, K.; Fang, X.; Lee, S.; Chen, X. *Mol. Pharm.* **2011**, *8*, 2331−2338.
(13) Kasten, B. B.; Jiang, K.; Cole, D.; Jani, A.; Udayakumar, N.; Gillespie, G. Y.; Lu, G.; Dai, T.; Rosenthal, E. L.; Markert, J. M.; Rao, J.; Warram, J. M. *Eur. J. Nucl. Med. Mol. Imaging* **2020**, *47*, 1412−1426.
(14) Chung, E. Y.; Ochs, C. J.; Wang, Y.; Lei, L.; Qin, Q.; Smith, A. M.; Strongin, A. Y.; Kamm, R.; Qi, Y.-X.; Lu, S.; Wang, Y. *Nano Lett.* **2015**, *15*, 5025−5032.
(15) Tannous, B. A.; Kim, D.-E.; Fernandez, J. L.; Weissleder, R.; Breakefield, X. O. *Mol. Ther.* **2005**, *11*, 435−443.
(16) Wurdinger, T.; Badr, C.; Pike, L.; de Kleine, R.; Weissleder, R.; Breakefield, X. O.; Tannous, B. A. *Nat. Methods* **2008**, *5*, 171−173.
(17) Tannous, B. A.; Kim, D.-E.; Fernandez, J. L.; Weissleder, R.; Breakefield, X. O. *Mol. Ther.* **2005**, *11*, 435−443.
(18) Kandoi, G.; Leelananda, S. P.; Jernigan, R. L.; Sen, T. Z. *Methods Mol. Biol.* **2017**, *1484*, 35−44.
(19) Zhai, Y.; Hotary, K. B.; Nan, B.; Bosch, F. X.; Muñoz, N.; Weiss, S. J.; Cho, K. R. *Cancer Res.* **2005**, *65*, 6543−6550.
(20) Van Meter, T. E.; Broaddus, W. C.; Rooprai, H. K.; Pilkington, G. J.; Fillmore, H. L. *Neurooncology* **2004**, *6*, 188−199.
(21) Sabeh, F.; Ota, I.; Holmbeck, K.; Birkedal-Hansen, H.; Soloway, P.; Balbin, M.; Lopez-Otin, C.; Shapiro, S.; Inada, M.; Krane, S.; Allen, E.; Chung, D.; Weiss, S. J. *J. Cell Biol.* **2004**, *167*, 769−781.

https://doi.org/10.1021/acs.analchem.0c05189
Anal. Chem. 2021, 93, 8739−8745